Hot corrosion in gas turbine components

N. Eliaz [a,*,1], G. Shemesh [b], R.M. Latanision [a]

[a] *H.H. Uhlig Corrosion Laboratory, Massachusetts Institute of Technology, Cambridge, MA 02139-4307, USA*
[b] *Metallurgical Laboratory, Israel Air Force, PO Box 02745, Israel*

Abstract

The macroscopic and microscopic characteristics as well as the proposed mechanisms of Type I (high-temperature) and Type II (low-temperature) hot corrosion are reviewed. Two case histories of gas turbine blade failures are presented. Different practical approaches to minimize hot corrosion are described. © 2002 Elsevier Science Ltd. All rights reserved.

Keywords: Corrosion; Oxidation; Turbine blade failures; Failure analysis; Fatigue failure

1. Introduction

Advances in material development and cooling schemes will lead to increased operation temperatures of new-generation gas turbine engines. The combination of such high temperatures with an aircraft environment that contains contaminants such as sodium, sulfur, vanadium, and various halides requires special attention to the phenomenon of hot corrosion. This form of corrosion, unlike oxidation, can consume the material at an unpredictably rapid rate. Consequently, the load-carrying ability of the component is reduced, leading eventually to its catastrophic failure. The inability to either totally prevent hot corrosion or at least detect it at an early stage has resulted in several aircraft accidents, leading to loss of life and/or destruction of engines. Several papers have already reviewed the characteristics and mechanisms of hot corrosion as well as the different approaches to combat it (see, for example, Refs. [1–6]).

At the beginning of the 1990s, a project was initiated at the Israel Air Force (IAF) aimed towards increasing the awareness of the maintenance teams to the problem of hot corrosion and developing technical instructions to prevent it. Consequently, failures due to hot corrosion have been minimized, in spite of the relatively aggressive marine environment to which Israeli aircraft are exposed. The objective of this paper is threefold: (1) to review the macroscopic and microscopic characteristics as well as the proposed mechanisms of hot corrosion; (2) to summarize the practical approaches to prevent hot corrosion; and (3) to present case histories of gas turbine blade failures due to hot corrosion.

* Corresponding author. Tel.: +1-617-253-5260; fax: +1-617-253-8745.
 E-mail address: neliaz@mit.edu (N. Eliaz).
 [1] Formerly at the Metallurgical Laboratory, Israel Air Force.

2. The gas turbine engine

Before dealing specifically with hot corrosion-related issues, it is appropriate to give a brief description of the system of interest in this work — the gas turbine engine. A more detailed description of this system and its components can be found elsewhere (e.g. in Refs. [7–13]).

Gas turbine engines, also known as jet engines, power most modern civilian and military aircraft. Fig. 1 shows a section of such an engine. The inlet (also known as intake), not shown in this figure, directs outside air into the engine. At the exit of the inlet is the compressor (marked as *a* in Fig. 1). In order to produce thrust, it is essential to compress the air before fuel is added. In an axial-flow compressor, such as the one shown in Fig. 1, the air flows in the direction of the shaft axis through alternate rows of stationary and rotating blades, called stators and rotors, respectively. Modern axial-flow compressors can increase the pressure 24 times in 15 stages, with each set of stators and rotors making up a stage [12]. The compressors in most modern engines are divided into low-pressure and high-pressure sections which run off two different shafts. In the combustor, or burner (*b* in Fig. 1), the compressed air is mixed with fuel and burned. Fuel is introduced through an array of spray nozzles that atomize it. An electric igniter is used to begin combustion. The combustor adds heat energy to the air stream and raises its temperature (up to about 1930°C), a process which is accompanied by a slight decrease in pressure (∼1–2%) [11]. For best performance, the combustion temperature should be the maximum obtainable from the complete combustion of the oxygen and the fuel. However, turbine inlet temperatures currently cannot exceed about 1100°C because of materials limits [12]. Hence, only part of the compressed air is burned in the combustor; the remainder is used to cool the turbine.

Leaving the combustor, the hot exhaust is passed through the turbine (*c* in Fig. 1), in which the gases are partially expanded through alternate stator and rotor rows. Depending on the engine type, the turbine may consist of one or several stages. Like the compressor, the turbine is divided into low-pressure and high-pressure sections, the latter being closer to the combustor. The turbine provides the power to turn the compressor, to which it is connected via a central shaft, as well as the power for the fuel pump, generator, and other accessories. From thermodynamics, the turbine work per mass airflow is equal to the change in the specific enthalpy of the flow from the entrance to the exit of the turbine. This change is related to the temperatures at these points. The temperature at the entrance to the turbine can be as high as 1650°C [13], considerably above the melting point of the material from which the blades are made. Therefore, to keep the turbine blades from melting, both complex cooling schemes and coatings are often used.

The gases, leaving the turbine at an intermediate pressure, are finally accelerated through a nozzle (not shown in Fig. 1) to reach the desired high jet-exit velocity. Because the exit velocity is greater than the free stream velocity, thrust is produced. The amount of thrust generated depends on the rate of mass flow through the engine and the leaving jet velocity, according to Newton's Second Law. Thus, the gas is
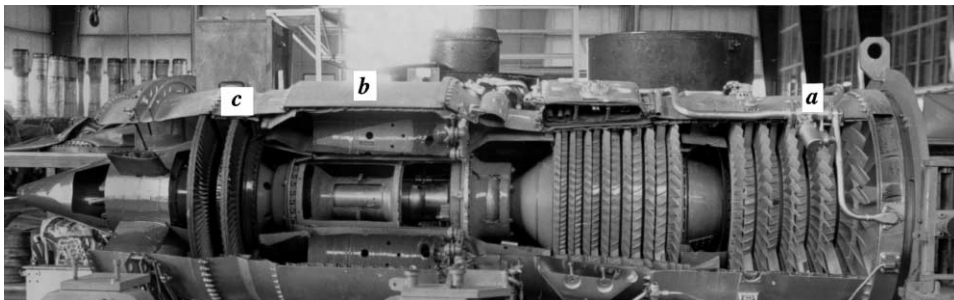

Fig. 1. Section of a gas turbine engine.

accelerated to the rear, and the engine (as well as the aircraft) is accelerated in the opposite direction according to Newton's Third Law.

With regard to hot corrosion, several local operating conditions in the engine are important. First, superalloys at turbines serve most time under an oxidizing environment. However, during ignition, a local reducing environment may form due to incomplete burning of fuel. Such a reducing atmosphere can damage the protective surface oxide layer, especially in the presence of contaminants such as Na_2SO_4. Second, hot corrosion is more frequently observed in the low-pressure turbine (LPT) than in the high-pressure turbine (HPT). This is because at the lower temperatures involved in LPT, corrosive contaminants are more likely to accumulate on the surface in significant amounts and/or for a greater percentage of time. Third, hot corrosion is usually greatest at the hottest point on the pressure (concave) surface of the turbine blade; at about midway along the length of the blade, and a short distance back from the leading edge [2].

3. Hot corrosion — definition

Hot corrosion may be defined as *accelerated* corrosion, resulting from the presence of salt contaminants such as Na_2SO_4, NaCl, and V_2O_5 that combine to form *molten* deposits, which damage the protective surface oxides.

4. Characteristics of hot corrosion

Hot corrosion is often divided into two forms of attack: Type I (or high-temperature hot corrosion), and Type II (or low-temperature hot corrosion). Various parameters may affect the development of these two forms, including alloy composition and thermomechanical condition, contaminant composition and flux rate, temperature and temperature cycles, gas composition and velocity, and erosion processes.

4.1. Type I hot corrosion (HTHC)

This form of hot corrosion is observed mainly within the temperature range 850–950°C [3,14]. HTHC starts with the condensation of fused alkali metal salts on the surface of the component. A cycle of subsequent chemical reactions takes place, initially attacking the protective oxide film and progressing to deplete the chromium element from the substrate material. With chromium depletion, oxidation of the base material accelerates and porous scale begins to form. The dominant salt in HTHC is Na_2SO_4 due to its high thermodynamic stability. The most significant source of sodium is marine atmosphere (sea salts contain Na_2SO_4 and NaCl), but it can also be found in industrial atmospheric pollutants and in volcanic discharges, as well as in the fuel. During combustion, sodium sulfate can form from sodium and sulfur, the latter being present in the fuel. Other impurities either in the fuel or in the air, such as vanadium, phosphorus, lead and chlorides, can combine with sodium sulfate to form a mixture of salts with a lower melting temperature, thus broadening the range of attack. For example, the melting point of Na_2SO_4 (884°C) can be lowered by the addition of NaCl, as an eutectic is formed with a melting point of about 620°C [3]. Furthermore, in combustion gases, NaCl itself will react with sulfur oxide and oxygen, forming Na_2SO_4 via the following reaction [15,16]:

$$2NaCl + SO_2 + O_2 \ \rightarrow \ Na_2SO_4 + Cl_2 \tag{1}$$

The presence of sodium chloride removes the incubation period, which otherwise is typical of HTHC [2,3]. Potassium sulfate (K_2SO_4) behaves similarly to sodium sulfate with regard to HTHC. Therefore, the definition of alkalis in the fuel or in the air often sums up the content of sodium and the content of potassium [14].

Vanadium is an unavoidable contaminant in certain liquid fuels. When vanadium-containing deposits cover components exposed to high temperatures, accelerated hot corrosion occurs. Extremely aggressive liquid phases of vanadium may form at temperatures as low as 535°C, depending on the ratio between Na and V [3]. In addition to their own relatively low melting point, the vanadium compounds markedly increase the solubility of the oxide when mixed with Na_2SO_4 [17].

HTHC can generally be divided into four progressive stages from initial onset to failure [18]:

1. In stage 1, slight roughening of the surface caused by some growth and localized breakdown of the oxide scale layer is evident. At this stage, neither chromium depletion in the substrate layer nor loss of mechanical integrity are observed.
2. In stage 2, the roughness of the surface is more marked as oxide layer breakdown continues. While chromium depletion commences at this stage, mechanical integrity is still not affected.
3. In stage 3, oxidation of the base material has penetrated to significant depth, with obvious build-up of scale. At this stage, mechanical integrity should be considered as jeopardized and the blades removed from service. Progression to stage 4 will accelerate with or without the continued presence of sodium.
4. In stage 4, catastrophic attack occurs. The attack penetrates deeply into the blade while forming a large 'blister' of scale. Failure is likely at this stage due to loss of structural material.

The macroscopic appearance of HTHC is characterized in many cases by severe peeling of the metal and by significant color changes (greenish tone, resulting from the formation of NiO) in the area of accelerated attack. Microscopically, the morphology of Type I is characterized by a sulfidation and depletion region beneath the porous, nonprotective, scale. The reaction products frequently exhibit oxide precipitates dispersed in the salt film [1].

4.2. Type II hot corrosion (LTHC)

This form of hot corrosion is observed mainly within the temperature range 650–800°C [2,3,19]. LTHC forms typical pitting, resulting from the formation of mixtures of Na_2SO_4 and $CoSO_4$ with low melting temperatures (the melting temperature of the Na_2SO_4–$CoSO_4$ eutectic is 540°C). $CoSO_4$ itself is a corrosion product of a reaction between the surfaces of blades made of cobalt-based alloys and SO_3 from the combustion gas. Similarly, the formation of Na_2SO_4–$NiSO_4$ eutectics has been suggested for nickel-based superalloys. Thus, a high partial pressure of SO_3 in the gaseous phase is required for the LTHC reactions to occur, in contrary to HTHC [14]. The localized nature of attack is related to localized failure of the scale as a result of local chloride attack, thermal cycling, or erosion. For example, salt may be trapped locally in crevices produced by scale cracking. Such deposits could be retained and allow local changes in salt composition to occur [3]. As opposed to Type I hot corrosion, in Type II neither incubation period nor microscopic sulfidation and chromium depletion are generally observed [3,20].

5. Mechanisms of hot corrosion

Several mechanisms have been suggested to explain the process of hot corrosion [1,2,21–26]. In this section, only a very brief summary will be presented. The initiation of HTHC is often attributed to failure of the protective oxide layer, which allows the molten salt to access directly the substrate metal. This failure may result from erosion, thermal stresses, erosion–corrosion, chemical reactions, etc. The mechanisms proposed for the HTHC propagation stage are the sulfidation–oxidation mechanism and the salt fluxing mechanisms [2]. The salt fluxing mechanism was originally proposed by Goebel and Pettit [21,22]. According to this model, the protection efficiency of the surface oxide layer might be lost as a result of fluxing of this layer in the molten salt. The fluxing can be caused either by combination of oxides with O^{2-}

to form anions (i.e. 'basic fluxing'), or by decomposition of oxides into the corresponding cations and O^{2-} (i.e. 'acidic fluxing'). Acidic fluxing takes place when the O^{2-} activity in the molten salt is markedly lowered; it leads to a much more severe oxidation compared to basic fluxing. As opposed to basic fluxing, acidic fluxing can be self-sustaining, since the displacement of the salt from stoichiometry does not become progressively more difficult as the reaction proceeds [2]. In general, hot corrosion of superalloys with high contents of aluminum and chromium (e.g. IN 738LC [27]) is often reported to occur according to the basic fluxing mechanism. On the other hand, hot corrosion of alloys with high contents of tungsten, molybdenum and vanadium is often reported to follow the acidic fluxing mechanism.

Rapp et al. measured the oxide solubilities in molten Na_2SO_4 as a function of the acidity of the salt. Based on these measurements, it was suggested [23] that a negative gradient of the solubility of the protective oxide in the salt film at the oxide/salt interface should lead to oxide dissolution at this interface and to precipitation of a non-protective oxide away from the interface, where the solubility is lower. Fluxing arises in this case only because of the local variation of sodium oxide activity and/or oxygen partial pressure across the salt film; no sulfide-forming reaction is necessary. This mechanism can explain a self-sustaining process of dissolution of the protective oxide to maintain an accelerated corrosion rate [2].

The effect of vanadium on HTHC has been explained by different researchers. Bornstein et al. [28] and Goebel et al. [26] suggested that a self-sustained acidic dissolution of the protective Cr_2O_3 or Al_2O_3 scales could occur when the salt film contains vanadium, because V_2O_5 is a strongly acidic oxide. Zhang and Rapp [29] suggested that every oxide should form an acidic solute with much higher solubility in the presence of vanadate, which should contribute to the more rapid attack of oxides by mixed sulfate–vanadate melts than by a pure sulfate melt.

A common model for the occurrence of LTHC was suggested by Luthra [30]. According to this model, LTHC follows two stages: (1) formation of liquid sodium–cobalt sulfate on the surface; and (2) propagation of attack via migration of SO_3 and cobalt inward and outward, respectively, through the liquid salt. Shih et al. [31] suggested sulfidation as the mechanism of LTHC in nickel-based alloys.

6. Laboratory testing techniques

Different tests have been developed to determine the resistance of alloys against hot corrosion. These include the crucible, electrochemical, accelerated oxidation, burner-rig, and pressurized burner-rig tests [25]. Most conditions in a gas turbine can be accurately simulated in a low-velocity burner-rig, with the exception of gas velocity and pressure [32]. Simmons et al. [33], however, suggested that hot corrosion is an electrochemical process in which the molten salt acts as an electrolyte. Since then, electrochemical tests have been widely used, either to measure hot corrosion rates or to study reaction mechanisms [1,6,34–39].

7. Prevention approaches

Several approaches have been employed to control hot corrosion of gas turbine components. These approaches include proper selection of structural alloys, application of coatings, washing of hot parts, air filtering, and control of both fuel cleanliness and composition.

7.1. Alloy selection

The resistance of superalloys (and other materials) against hot corrosion is directly related to the chemical composition of the alloy and its thermomechanical history. Unfortunately, many alloying elements have an adverse effect on the mechanical properties of the superalloy at high temperatures and on its

resistance to hot corrosion. For example, elements such as tungsten, vanadium and molybdenum are excellent in improving the mechanical properties, but their presence makes the alloy highly susceptible to hot corrosion [2,25]. Therefore, a tradeoff in material selection is often made, and protective coatings are chosen as a major means to provide hot corrosion resistance (see Section 7.2).

Chromium is the most effective alloying element for improving the hot corrosion resistance of superalloys [40]. In order to attain good resistance to HTHC, a minimum of 15 wt.% Cr is often required in nickel-based alloys, and a minimum of 25 wt.% Cr in cobalt-based superalloys [2]. IN 713C, IN 100 [2] and CM 247LC [6] represent the alloys where this criterion is not fulfilled; therefore, they are very susceptible to HTHC. On the other hand, IN 738LC and X-40 have been used to manufacture both stators and rotors [2,41]. The chemical composition of these alloys is given in Table 1. The positive effect of chromium on the HTHC resistance is usually attributed to the reaction of Cr_2O_3 to stabilize the melt chemistry (e.g. by forming a stable Na_2CrO_4 solute), thus preventing dissolution/reprecipitation of the protective oxide scale [26,28,42]. One should note, however, that high content of chromium would lead to the formation of TCP phases, which decrease the strength and ductility of the alloy at high temperatures [25].

The effect of other alloying elements on the hot corrosion resistance of superalloys has been reported as well. Cerium, lanthanum, zirconium, yttrium, and scandium significantly increase the resistance as they improve the adhesion between the alloy and the protective oxide [25]. Silicon, platinum, and hafnium have all been shown to have beneficial effects, at least on LTHC resistance. Titanium, aluminum, and niobium were found [27] to increase the hot corrosion resistance.

Cobalt-based superalloys are, in general, more resistant to HTHC than nickel-based superalloys. This may result from the higher melting temperature of $Co–Co_4S_3$ eutectic (877°C) in comparison to $Ni–Ni_3S_2$ eutectic (645°C). In addition, the diffusivity of sulfur in cobalt alloys is approximately 100 times lower than in nickel alloys [25]. Cobalt-based superalloys, however, are more susceptible to LTHC than nickel-based alloys.

The microstructure of the alloy is another important factor. Secondary phases might lead to an accelerated attack, either along phase boundaries or by selective attack of one phase. In particular, it is important to avoid coarse refractory metal carbides [2].

7.2. Protective coatings

This is the preferred approach, even when relatively hot corrosion-resistant base alloys are used. The numerous variants of high-temperature coatings that are in use today may be categorized into three generic types: diffusion, overlay, and thermal barrier coatings.

Diffusion coatings are formed by the surface enrichment of an alloy with either aluminum, chromium, or silicon. Aluminide coatings that have been specified for engine service include PWA70 and MDC3V (fabricated by pack chromized), PWA62 (two-step pack chromized and pack aluminized), TEW LDC2 and Chromalloy RT22 (Pt-electroplated coating and pack aluminized), Elbar Elcoat 360 (Ti/Si slurry

Table 1
Nominal compositions (wt.%) of superalloys discussed in this paper

Alloy	Ni	Co	Cr	Ti	Al	Mo	W	Ta	Hf	Zr	C	B	V	Nb	Fe	Mn	Si
CM 247LC	Bal.	9.2	8.1	0.7	5.6	0.5	8.5	3.20	1.4	0.015	0.05	0.015	–	–	–	–	–
IN 100	Bal.	15.0	10.0	5.0	5.5	3.0	–	–	–	0.060	0.18	0.010	1.0	–	–	–	–
IN 713C	Bal.	–	12.5	0.8	6.0	4.2	–	1.75	–	0.100	0.12	0.012	–	0.9	–	–	–
IN 738LC	Bal.	8.5	16.0	3.4	3.4	1.7	2.6	1.70	–	0.050	0.11	0.011	–	0.9	–	–	–
MAR-M200	Bal.	10.0	9.0	2.0	5.0	–	12.5	–	–	0.050	0.15	0.015	–	1.0	1.0	–	–
X-40	10.0	Bal.	22.0	–	–	–	7.5	–	–	–	0.50	–	–	–	1.5	0.5	0.5

diffusion), etc. [19]. The addition of platinum to aluminide coatings has been found to increase the resistance against cyclic oxidation at high temperatures ($>1000°C$) due to formation of a more adherent protective alumina layer and delay of the formation of spinel during oxidation exposure [5,43].

Overlay coatings are a family of corrosion-resistant alloys specifically designed for high-temperature surface protection. They are often referred to as M–Cr–Al–Y coatings, where M is the alloy base metal (typically nickel, cobalt, or a combination of these two). The high-chromium low-aluminum M–Cr–Al–Y coatings typically resist LTHC attack, while lower chromium and higher aluminum contents are typically required for HTHC resistance. Recently, other oxygen-active alloying elements have also been added to these coatings. For example, PWA286 is a patented overlay by Pratt & Whitney containing Ni, Co, Cr, Al, Hf, Si, and Y. These more complex alloy systems are often known as M–Cr–Al–X or M–Cr–Al–X–Y coatings, where X denotes elements other than yttrium. Typical commercial overlay coatings include Co–23Cr–12Al–0.5Y, Co–32Ni–21Cr–8Al–0.5Y, and PWA270 [5,19,44].

Thermal barrier coatings (TBCs) are designed to insulate the substrate from the heat of the gas flow. They are a composite coating system consisted of an outer ceramic coating (usually stabilized zirconia) overlaid on an oxidation-resistant bond coat. The bond coat is typically an M–Cr–Al–Y overlay coating or a diffusion aluminide coating [5,19]. One should note that the application of TBCs in gas turbines that serve under sea atmosphere and in diesel engines is very limited because yttria (Y_2O_3), magnesia (MgO) and calcia (CaO), the commonly used stabilizers for zirconia-based TBCs, react with sulfur, sodium and vanadium contaminants [45,46]. Yet, the life of such coatings may be extended by post-laser treatment [45].

Recently, a smart coating that is resistant to both HTHC and LTHC was developed. This smart coating is a functionally graded overlayer coating produced using a combination of plasma-spray and diffusion techniques. It contains a high-chromium-enriched region midway through the coating, which limits LTHC pitting attack, and is overcoated with a β-aluminide-rich zone to provide high-temperature oxidation resistance and resistance to HTHC. The smart coating was reported to match the performance of the best HTHC-resistant RT22 coating (a platinum aluminide) and LTHC-resistant Sermetal 1515 diffusion coatings (a triple-cycle silicon aluminide treatment) [19].

Nowadays, there is a growing interest in using intermetallic compounds to manufacture blades for gas turbine engines. Hence, the application of protective coatings on such materials has been studied as well. Vacuum arc deposited Ni–Cr–Al–Y–Si was found [47] to provide Ni_3Al-based IC-6 cast alloy with an effective protection against oxidation and hot corrosion. Ti–Al–Cr coatings were reported [47,48] to provide good protection to γ-TiAl base alloys. An enamel coating was also found [49] to be very effective in protecting TiAl-based alloys against hot corrosion attack.

7.3. Washing of hot components

A proven approach to minimize hot corrosion is deluge motoring washes using plain water [2,18]. This allows for dissolving and carrying away salts and other contaminants, thus preventing the initiation of hot corrosion. Specific washing procedures are usually covered in detail in the relevant maintenance manual for the engine model concerned. Washing may be required either before each flight or up to once a month, depending on the estimation of the severity of the corrosion environment. An alternative method of establishing wash frequency has been to monitor blade condition using a borescope inspection program, adjusting the wash schedule according to the inspection results [18].

7.4. Air filtering

A limiting level of 0.008 ppm (by weight) has been suggested for the content of Na in the air, below which hot corrosion will not exist. Therefore, secondary protection against hot corrosion may be attained by installation of high-efficiency air filters [2,44].

7.5. Fuel cleanliness and composition

Fuel cleanliness affects the initiation and propagation of hot corrosion attack. Hence, the content of the alkali metal, vanadium, and sulfur in the fuel should be carefully controlled [2]. Sometimes, the maximal content of impurities allowed in the fuel is defined as 0.2–0.6 ppm (Na + K), 0.5 ppm V, and 1% S. However, these limits may change if a coating is applied on the blade and/or inhibitors are added to the fuel [50].

Often, additives are added to the fuel; additions of Mg, Cr, Ca, and Ba decrease the corrosion rate [2]. If high levels of vanadium are to be used in the fuel, its effect can be combated by MgO additions. The effect of magnesia is to react preferentially with vanadium pentoxide (V_2O_5) to form $Mg_3V_2O_8$ vandates with higher melting temperature [3]. Zinc, added by means of protective coatings or anodes in the fuel tank, is effective in reducing LTHC attack. In the absence of excess NaCl, zinc decreases the solubility of the protective metal oxides in the salt and the electrochemical potential of the corrosion reaction. In the presence of excess NaCl, zinc (rather than other metals from the protective oxide layer) reacts easily with the chloride ion; simultaneously, it serves as a mean of transferring the chloride to the salt-gas interface, where it is transformed to chlorine gas via sulfitation reaction [51].

8. Case histories

In this section, two case histories of turbine blade failures due to hot corrosion are presented.

8.1. Case history #1

Two stage I blades from a PT6 engine were inspected in the lab. Loss of material at the top of the blade, distortion — mainly about midway along the length of the blade, and color changes on the concave surface, were visually observed. Longitudinal cross-section was prepared about 6.4 mm (0.25 inch) from the trailing edge, as common for certain over-temperature inspections. Fig. 2a shows the typical macrostructure about midway along the length of the blade. Porous scales and 'spikes' are evident. Bright gray particles are evident beneath the inner scale layer. Using SEM/EDS analysis, these particles were found to be sulfide precipitates. The chemical composition of the base alloy was in accordance with MAR-M200 (see Table 1), which is relatively susceptible to hot corrosion. No cracks typical of creep were observed. After chemical etching (Fig. 2b), no evidence of microstructural changes along the blade was identified. Hence, an over-temperature event could be eliminated as well. The bright layer around the 'spikes' was found (SEM/EDS) to be enriched with aluminum and tungsten and depleted from nickel and cobalt. Traces of chlorine, sulfur and potassium were found in the scale. Based on the aforementioned observations, it was concluded that the blades suffered from hot corrosion attack. Thus, all stage I blades in this engine were replaced, and washing operations were re-examined.

8.2. Case history #2

A severely damaged turbine blade was inspected in the lab. Macroscopic inspection indicated the loss of a large piece of blade near the leading edge, at about 1.7 cm from the top of the blade (Fig. 3a). A long crack, about 4.6 mm in length, was found to propagate from this region into the material (Fig. 3b). The crack was then opened at the lab. Inspection of the fracture surface under an SEM (i.e. fractography) revealed fatigue striations, propagating from the leading edge of the blade. Striation analysis indicated the occurrence of high-cycle low-stress fatigue. A transverse metallographic cross-section was prepared through the origin of the crack, perpendicular to the fracture surface, and inspected under an optical microscope. A relatively advanced hot corrosion attack was observed (Fig. 3c), with oxidation penetrating
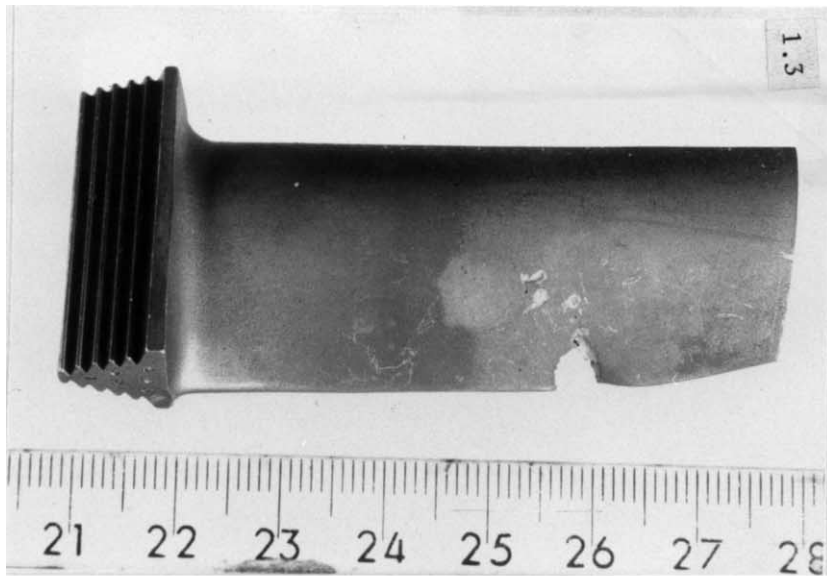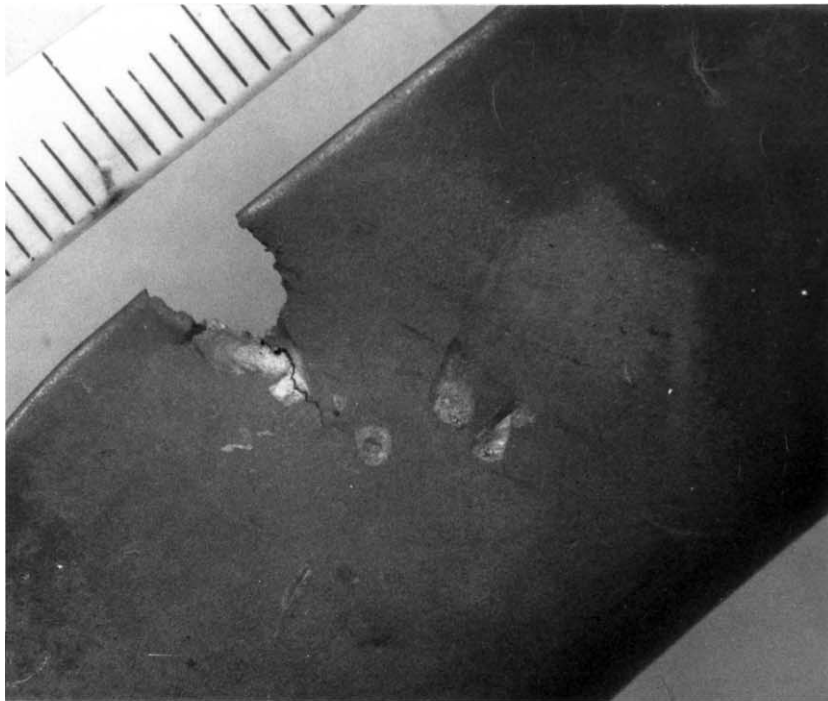
25 μm

(a)

50 μm
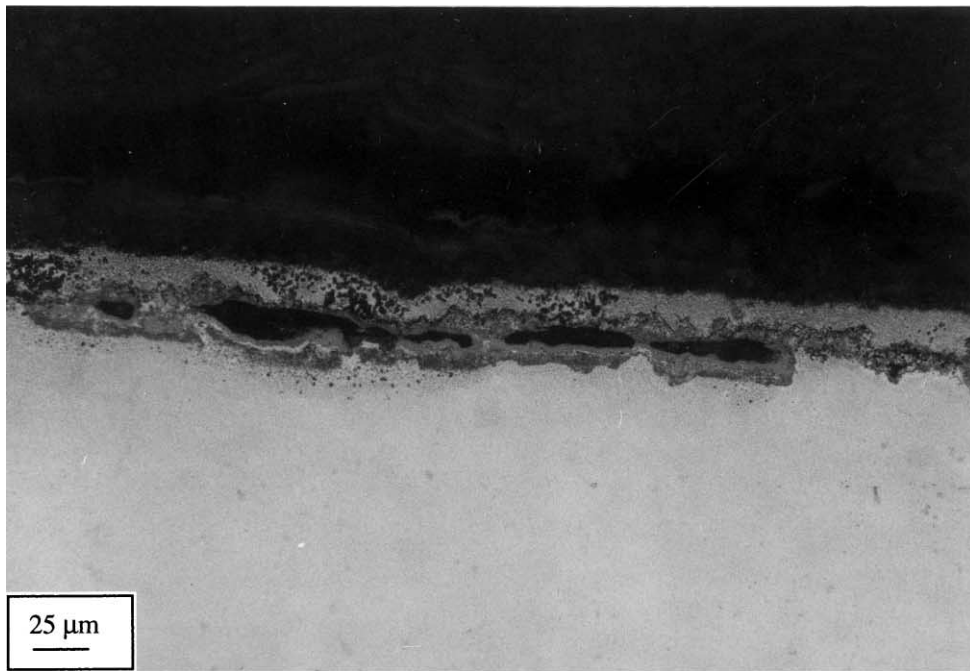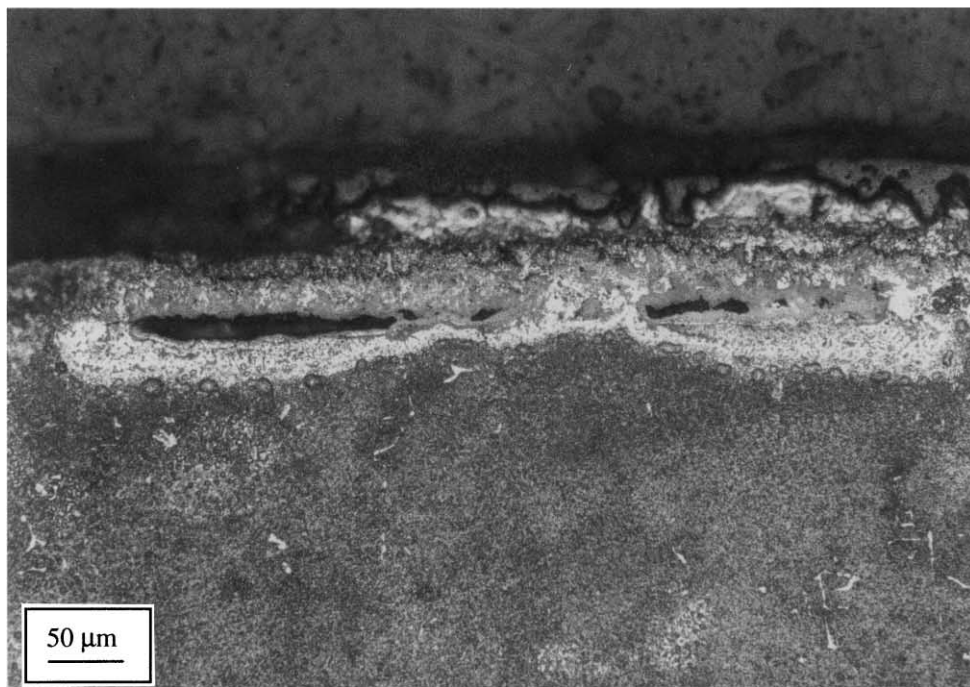
(b)

Fig. 2. Optical micrographs indicating hot corrosion in stage I turbine blades from a PT6 engine, (a) before and (b) after chemical etching.
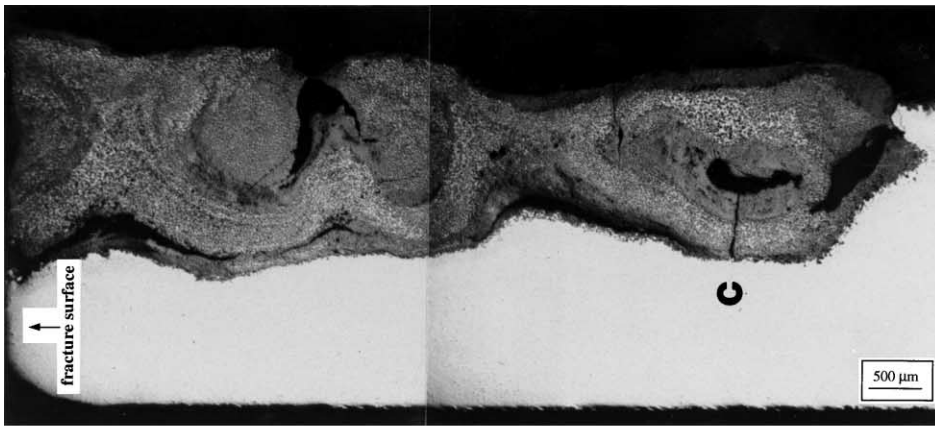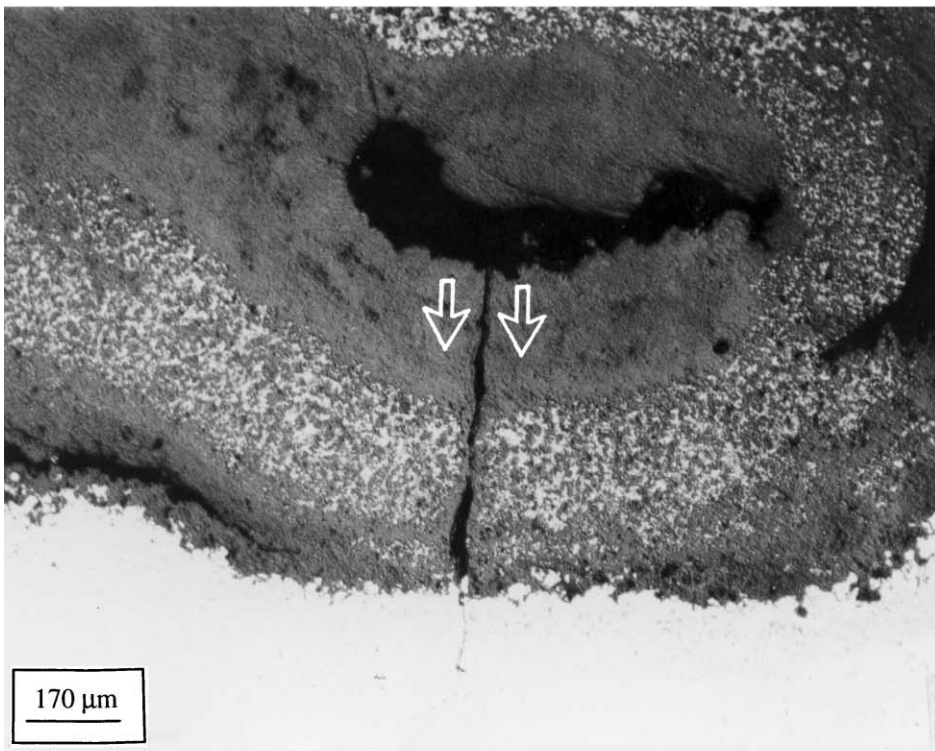
(a)

(b)

Fig. 3. (a) Macroscopic view of a turbine blade, indicating the loss of a large piece of material near the leading edge; (b) a crack propagating into the remainder material; (c) optical micrograph indicating advanced hot corrosion attack; and (d) a secondary crack propagating from the scale into the base material, in parallel to the main fracture surface.

(c)

(d)

Fig. 3   *(continued)*

deeply into the blade (up to about 0.8 mm). This high penetration depth, combined with large blisters and eddies within the scale, indicate that the hot corrosion had already progressed to Stage 4 (see Section 4). In addition, a secondary crack was found to propagate from the scale into the base material, in parallel to the main fracture surface (Fig. 3d). A similar crack could ultimately propagate to catastrophic failure under fatigue mechanism. SEM/EDS analysis identified the blade material as cast IN 713C, known for its susceptibility to hot corrosion (see Section 7.1).

Based on the aforementioned observations, it was concluded that the blade failed as a result of crack propagation under low stresses of vibrations. The origin of the fatigue crack was a preliminary crack (or flaw), formed as a result of advanced hot corrosion attack. Thus, the recommendations of this investigation included replacement of all turbine blades and re-examination of all washing and monitoring operations.

9. Conclusions

1. Hot corrosion is a failure mechanism of great concern in gas turbine engines. The hot corrosion process must be either totally prevented or detected at an early stage to avoid catastrophic failure.
2. Based on different characteristics and mechanisms, it is possible to distinguish between high-temperature hot corrosion (HTHC, or Type I hot corrosion) and low-temperature hot corrosion (LTHC, or Type II hot corrosion).
3. The ultimate failure of turbine blades may result from a combination of hot corrosion and another failure mechanism (e.g. fatigue).
4. Application of a proper combination of preventive approaches should lead, in practice, to a significant decrease in the number of failures due to hot corrosion.

References

[1] Rapp RA. Chemistry and electrochemistry of the hot corrosion of metals. Corrosion 1986;42(10):568–77.
[2] Stringer J. High-temperature corrosion of superalloys. Mater Sci Technol 1987;3(7):482–93.
[3] Hancock P. Vanadic and chloride attack of superalloys. Mater Sci Technol 1987;3(7):536–44.
[4] Tzvetkoff TZ, Girginov A, Bojinov M. Corrosion of nickel, iron, cobalt and their alloys in molten salt electrolytes: review. J Mater Sci 1995;30(22):5561–75.
[5] Goward GW. Progress in coatings for gas turbine airfoils. Surf Coat Technol 1998;108-109(1-3):73–9.
[6] Gurrappa I. Hot corrosion behavior of CM 247 LC alloy in Na_2SO_4 and NaCl environments. Oxid Met 1999;51(3–4):353–82.
[7] Fawley RW. Superalloy progress. In: Sims C.T., Hagel W.C., editors. The superalloys. New York: Wiley, 1972. p. 3–29.
[8] Endres W. Design principles of gas turbines. In: Sahm P.R., Speidel M.O., editors. High-temperature materials in gas turbines. Amsterdam: Elsevier, 1974. p. 1–14.
[9] Driver D, Hall DW, Meetham GW. The gas turbine engine. In: Meetham G.W., editor. The development of gas turbine materials. London: Applied Science Publishers, 1981. p. 1–30.
[10] Desforges CD. Metals and alloys for high temperature application: current status and future prospects. In: Bradley F., editor. Source book on materials for elevated-temperature applications. Metals Park: ASM, 1979. p. 1–18.
[11] Animated jet engine part. http://www.lerc.nasa.gov/WWW/K-12/airplane/animation/turbpar/entb.html
[12] Pratt & Whitney home page. http://www.pratt-whitney.com
[13] Engine terminology. http://www.pratt-whitney.com/engines/terminology.html
[14] Wright IG. High-temperature corrosion. In: Metals handbook, vol. 13. 9th ed. Metals Park: ASM, 1987. p. 97–103.
[15] Jaffee RI, Stringer J. High-temperature oxidation and corrosion of superalloys in the gas turbine (a review). In: Bradley F., editor. Source book on materials for elevated-temperature applications. Metals Park: ASM, 1979. p. 19–33.
[16] Santorelli R, Sivieri E, Reggiani RC. High-temperature corrosion of several commercial Fe–Cr–Ni alloys under a molten sodium sulphate deposit in oxidizing gaseous environments. Mater Sci Eng A 1989;A120:283–91.
[17] Rapp RA, Zhang YS. Hot corrosion of materials — fundamental studies. JOM 1994;46(12):47–55.
[18] Pratt & Whitney. Sulphidation attack. S.I.L. no. 1035, 3017, 4010, 5028, 7022, 11008, 12020, 13011, October 1987.
[19] Nicholls JR. Designing oxidation-resistant coatings. JOM 2000;52(1):28–35.
[20] Meier GH. A review of advances in high-temperature corrosion. Mater Sci Eng A 1989;120:1–11.
[21] Goebel JA, Pettit FS. Na_2SO_4-induced accelerated oxidation (hot corrosion) of nickel. Metall Trans 1970;1:1943–54.
[22] Goebel JA, Pettit FS. The influence of sulfides on the oxidation behavior of nickel-base alloys. Metall Trans 1970;1:3421–9.
[23] Zhang JS, Hu ZQ, Murata Y, Morinaga M, Yukawa N. Design and development of hot corrosion-resistant nickel-base single-crystal superalloys by the d-electrons alloy design theory; II: effects of refractory metals Ti, Ta, and Nb on microstructures and properties. Metall Trans A 1993;24A(11):2451–64.

[24] Rapp RA, Goto KS. The hot corrosion of metals by molten salts. In: Braunstein J., Selman J.R., editors. Proceedings of the Second International Symposium on Molten Salts, vol. 81-10. Pennington: The Electrochemical Society, 1981. p. 159–77.

[25] Otsuka N, Rapp RA. Hot corrosion of preoxidized Ni by a thin fused Na_2SO_4 film at 900°C. J Electrochem Soc 1990;137(1):46–52.

[26] Beltran AM, Shores DA. Hot corrosion In: Sims CT, Hagel WC, editors. The superalloys. New York: Wiley, 1972. p. 317–39.

[27] Bornstein NS, DeCrescente MA, Roth HA. The relationship between relative oxide ion content of Na_2SO_4, the presence of liquid metal oxides and sulfidation attack. Metall Trans 1973;4:1799–810.

[28] Goebel JA, Pettit FS, Goward GW. Mechanisms for the hot corrosion of nickel-base alloys. Metall Trans 1973;4:261–78.

[29] Zhang YS, Rapp RA. Solubilities of CeO_2, HfO_2 and Y_2O_3 in fused Na_2SO_4–30 mol% $NaVO_3$ and CeO_2 in pure Na_2SO_4 at 900°C. Corrosion 1987;43(6):348–52.

[30] Luthra KL. Mechanisms of low temperature hot corrosion. In: Rapp RA, editor. High temperature corrosion. Houston: NACE, 1983. p. 507-18.

[31] Shih S, Zhang Y, Li X. Sub-melting point hot corrosion of alloys and coatings. Mater Sci Eng A 1989;A120:277–82.

[32] Nicholls JR, Saunders SR. Comparison of hot-salt corrosion behaviour of superalloys in high and low velocity burner rigs. High Temp Technol 1989;7(4):193–201.

[33] Simmons EL, Browning GV, Liebhafsky HA. Sodium sulfate in gas turbines. Corrosion 1955;11:505t–14t.

[34] Baudo G. Coatings Corrosion 1977;1:11–41.

[35] Gao G, Stott FH, Dawson JL, Farrell DM. Electrochemical monitoring of high-temperature molten-salt corrosion. Oxid Met 1990;33(1-2):79–94.

[36] Hara M, Shinata Y. Electrochemical studies on hot corrosion of Ni–Cr–Al alloys in molten Na_2SO_4–NaCl. Mater Trans JIM 1992;33(8):758–68.

[37] Kim JJ, Cho SM. Effects of galvanostatic treatments on hot corrosion of Ni. J Mater Sci Lett 1994;13(21):1573–6.

[38] Rahmel A. Electrochemical aspects of molten-salt-enhanced corrosion. Mater Sci Eng 1987;87:345–52.

[39] Baudo G, Tamba A, Bombara G. An electrochemical investigation of corrosion of ferritic steels in molten sulfates. Corrosion 1970;26(7):193–9.

[40] Otsuka N, Rapp RA. Effects of chromate and vanadate anions on the hot corrosion of preoxidized Ni by a thin fused Na_2SO_4 film at 900°C. J Electrochem Soc 1990;137(1):53–60.

[41] Zhang JS, Hu ZQ, Murata Y, Morinaga M, Yukawa N. Design and development of hot corrosion-resistant nickel-base single-crystal superalloys by the d-electrons alloy design theory; I: characterization of the phase stability. Metall Trans A 1993;24A(11):2443–50.

[42] Bornstein NS, DeCrescente MA. The role of sodium in the accelerated oxidation phenomenon termed sulfidation. Metall Trans 1971;2:2875–83.

[43] Dahotre NB. Functional coatings and their applications: a web perspective. JOM 2000;52(1):14.

[44] Nakamori M, Kayano I, Ysukuda Y, Takahashi K, Torigoe T. Hot corrosion and its prevention in high temperature heavy oil firing gas turbines. Mater Sci Forum 1997;251-254:633–40.

[45] Gurrappa I. Thermal barrier coatings for hot corrosion resistance of CM 247 LC superalloy. J Mater Sci Lett 1998;17(15):1267–9.

[46] Longa-Nava Y, Zhang YS, Takemoto M, Rapp RA. Hot corrosion of nickel–chromium and nickel–chromium–aluminum thermal-spray coatings by sodium sulfate–sodium metavanadate salt. Corrosion 1996;52(9):680–9.

[47] Huo X, Zhang JS, Li JP, Wu FJ, Han YF. Evaluation of NiCrAlYSi overlay coating on Ni_3Al based alloy IC-6 after an engine test. Surf Coat Technol 1999;114(2-3):174–80.

[48] Brady MP, Brindley WJ, Smialek JL, Locci IE. The oxidation and protection of gamma titanium aluminides. JOM 1996;48(11):46–50.

[49] Tang Z, Wang F, Wu W. Effect of Al_2O_3 and enamel coatings on 900°C oxidation and hot corrosion behaviors of gamma-TiAl. Mater Sci Eng A 2000;A276(1-2):70–5.

[50] Viswanathan R. Corrosion of combustion turbines. In: Metals handbook, vol. 13. 9th ed. Metals Park: ASM, 1987. p. 999–1001.

[51] Hancock PJ, Hancock HA, Caley WF. Hollingshead RS. A review of recent studies of the role of zinc as an inhiitor of hot corrosion from molten sulphates. Mater Sci Eng A 1989;A120:313–8.